Talanta 85 (2011) 136–141

Contents lists available at ScienceDirect

Talanta

journal homepage: www.elsevier.com/locate/talanta

In situ spectral imaging of marker proteins in gastric cancer with near-infrared and visible quantum dots probes

Yue He[a], Hao Xu[a], Chuang Chen[b], Jun Peng[a], Hongwu Tang[a,*], Zhiling Zhang[a], Yan Li[b], Daiwen Pang[a]

[a] Key Laboratory of Analytical Chemistry for Biology and Medicine (Ministry of Education), College of Chemistry and Molecular Sciences, Research Center for Nanobiology and Nanomedicine (MOE 985 Innovative Platform), and State Key Laboratory of Virology, Wuhan University, Wuhan, 430072, P. R. China
[b] Department of Oncology, Zhongnan Hospital of Wuhan University and Hubei Key Laboratory of Tumor Biological Behaviors, Wuhan, 430071, China

ARTICLE INFO

Article history:
Received 1 December 2010
Received in revised form 11 March 2011
Accepted 17 March 2011
Available online 30 March 2011

Keywords:
Quantum dots
Cancer biomarkers
Spectral images
Hadamard transform
Near-infrared fluorescence

ABSTRACT

This study presents the investigation of bioconjugating ability of near-infrared (NIR) CdSeTe/ZnS quantum dots (QDs) (710 nm) and visible CdSe QDs (595 nm) in immunofluorescent staining for cancer biomarkers in gastric cancer tissues probed with the homemade Hadamard transform (HT) spectral imaging microscope and a commercial multispectral imaging system. The results show that imunostaining ability of NIR QDs probes is stronger than that of visible QDs when the two kinds of QDs are simultaneously used to probe the cancer biomarkers such as cytokeratin 20 (CK20) and proliferating cell nuclear antigen (PCNA) in gastric cancer tissues. Moreover, when the two QDs probes are used for immunostaining successively for the same target molecules, staining order has great influences on the final results due to their different conjugating ability to the marker proteins. The results imply that NIR QDs hold more promise for real-time imaging of tumor tissues due to its higher sensitivity and contrast. In addition, the results also demonstrate the potential of Hadamard transform spectral imaging as a useful tool in biomedical analysis and quantitative evaluation for tumor tissues.

1. Introduction

Fluorescent semiconductor nanocrystals quantum dots (QDs) are nanoscale crystalline clusters (1–10 nm), which are quite suitable for applying as fluorescent probes for biomedical investigations. QDs have several unique photo-physical properties such as high quantum yield, strong fluorescence, wide excitation spectrum, narrow fluorescence emission peak, multiple-color emission with a single excitation and long fluorescence lifetime, as well as high optical and chemical stability. Studies of Bruchez et al. [1], Chan and Nie [2] have shown that QDs can be used as biological probes applicable to live cell systems. Recently QDs have achieved important results in the biomedical field [3–5]. Moreover, QDs as fluorescence probes bioconjugate with cancer biomarkers have highlighted its advantages [6–8].

While the fluorescence imaging with QDs has been mainly performed in the visible spectral region, biomedical fluorescence imaging, especially noninvasive *in vivo* imaging, requires deep penetration of light into and out of tissues. The penetration depth of light depends on the absorption and scattering properties of the tissue and the absorbance of water. The best penetration is achieved by light with a NIR wavelength ranging from 700 to 1400 nm [9], which is referred as the "diagnostic window" [10,11]. Up till now, most NIR fluorescence imaging has been done with conventional or recently synthesized NIR dye molecules having over 10% of quantum yield [12–14] such as cyanine and alexa fluorophore series [15,16]. However, NIR dyes have the same inherent limitations as visible dyes, namely, low fluorescence quantum yield, broad emission peaks, rapid photodegradation and narrow absorption spectra [17]. Therefore, NIR quantum dots holds great promise for real-time *in vivo* fluorescent imaging [11,18–22].

Gastric cancer is the second leading cause of cancer death worldwide. It is particularly common in Asia and especially in China and Japan [23,24]. Proliferating cell nuclear antigen (PCNA) and cytokeratins (CK) are molecular biomarkers, which can be used for diagnosis and prognosis of gastric cancer. PCNA acts as a process factor for DNA polymerase delta in eukaryotic cells, which is important for both DNA synthesis and DNA repairing [25,26]. PCNA is over-expressed in proliferative cells and objectively reflects the proliferative activity of tumor cells. Therefore, PCNA is widely used in prognosis and diagnosing the proliferation activity of tumor cells [27]. CK are proteins of keratin found in the intracytoplasmic cytoskeleton of epithelial tissues [28]. CK20 is commonly expressed in the gastrointestinal tract. In surgical pathology, the immunoassays of cytokeratins are widely used for various epithelial tumor diagnosis and characterization [29].

The Hadamard transform (HT), which is one of the most common mathematic transforms based on square waves, is well

* Corresponding author. Tel.: +86 27 68752439 8077; fax: +86 27 68754067.
E-mail address: hwtang@whu.edu.cn (H. Tang).

0039-9140/$ – see front matter © 2011 Elsevier B.V. All rights reserved.
doi:10.1016/j.talanta.2011.03.035

suited to multiplexed imaging [30]. In our previous reports, a system of HT microscopic fluorescence imaging which can generate 511×512 pixel image was developed using a movable mask and the system was applied to quantify the DNA content in single cells labeled with fluorescent dyes [31]. More recently, we developed a HT spectral imaging microscope and it was successfully applied to capture four-dimensional (4D) images for samples-location coordinate (X and Y), fluorescence intensity (Z) and wavelength or time to probe important intrinsic or extrinsic biomolecules in cells or tissues [32].

In this study, we used HT spectral imaging technique to investigate the difference bioconjugate efficiency on the cancer biomarkers in gastric cancer tissues between NIR CdSeTe/ZnS QDs and visible QDs probes, and a comparative study was performed with CRi Nuance multispectral imaging technique.

2. Experimental

2.1. Materials and apparatus

Formalin-fixed, paraffin-embedded (FFPE) gastric neoplasms and normal gastric tissue sections were obtained from Hubei Key Laboratory of Tumor Biological Behaviors and Zhongnan Hospital of Wuhan University and were cut into 4 μm sections for QDs-Abs profiling. All the gastric tissue samples were human female patients aged 50 ± 5, and collected in about one-week since their clinical recognition.

Water-soluble CdSeTe/ZnS QDs (emission wavelength ~710 nm and full-width at half-maximum ~68 nm) were purchased from Invitrogen Corporation (U.S.A.) and were used as NIR probes. The surface of the NIR QDs was functionalized with carboxyl group. Visible CdSe QDs emitting at 550 and 595 nm, which were provided by Wuhan Jiayuan Quantum Dots Co., Ltd., were also used as fluorescent probes (FWHM < 30 nm). QDs probes with fluorescence peaks at 550, 595 and 710 nm were prepared after streptavidin was used to conjugate the above three kinds of QDs. Therefore, QDs coupled to streptavidin (QDs-SA) were used as probes immunostaining cancer-marker proteins in this study. Mouse anti-human CK antibody, mouse anti-human PCNA antibody and biotin tagged goat anti-mouse IgG were purchased from Fuzhou MaiXin. Bio. (Fuzhou, China).

The microscopic fluorescence spectra and fluorescence images of the specimens were obtained from the homemade HT fluorescence spectral imaging microscope in our laboratory. The details of the HT imaging microscope have been described in our previous work [32]. The HT fluorescence images and spectra for the tissue sections were captured by a 25×0.65 NA objective throughout the experiment. For acquiring fluorescence spectra and fluorescence imaging the QDs labeled specimens were illuminated with a defocused Argon Laser (35LAP 431, Melles Griot, USA) at 488 nm (4 mW, 4.2×10^3 W/m^2) throughout the experiment. Fluorescence micrographs were captured by DP72 microscope digital camera equipped to a BX51 microscope (Olympus Optical Co., Tokyo, Japan) with blue light from a mercury lamp illuminating the specimens. Digital photos were captured under the same condition with a 10× objective.

Image cubes were captured by CRi's (Cambridge Research & Instrumentation, Inc.) Nuance multispectral imaging system, which consists of an optical head, which was installed on a BX51 (Olympus Optical Co., Tokyo, Japan) microscope's C-mount camera port that includes a liquid crystal tunable filter (LCTF, bandwidth of 20 nm, scanning wavelength range of 500–950 nm) with a spectrally optimized lens system that relays the image to a scientific-grade megapixel CCD. The tunable filter automatically steps in 10 nm increments from 420 to 720 nm while the camera capturing images at each wavelength with 400 ms exposure. The resuled TIFF images (spectral cube, containing the spectra of all pixels) were loaded into the software (Nuance 2.8.0) for further analysis. The software can be used to quantitatively measure the total QD signal (S) and the corresponding area (A) of each unmixing spectral image cube. In this study we use the ratio of S (counts) and A (pixels) to measure the bioconjugation efficiency of QDs for cancer biomarkers.

2.2. Method

NIR QDs are coupled to marker proteins CK and PCNA indirectly through the biotin–streptavidin system. The QDs labeling operation follows the standard protocol of the kit. Mouse anti-human PCNA/CK antibodies are used to connect PCNA/CK in the cell nucleus/membranes, and biotin tagged goat anti-mouse IgG was used to connect the probes of QDs-SA and the mouse anti-human PCNA or CK antibody, respectively. In this experiment, when tissue sections were labeled, visible SA-CdSe QDs were added into the NIR SA-CdSeTe solution and served as indicators for the locations of the lesions.

The specimens were labeled with mixed use of red QDs in visible region and NIR QDs conjugating CK or PCNA. Through the comparison between fluorescence micrographs or the microscopic fluorescence spectra of the visible QDs, NIR QDs and the mixed QDs solution of the two, the labeling ability between the red visible QDs and the NIR QDs were compared. In addition, the same biomarker was labeled repeatedly by using 710 nm QDs and 595 nm QDs to investigate the influence on the multicolor labeling caused by the adding order of different QDs. First, two adjacent sections of a same tissue were stained with excessive 595 nm QDs which are coupled to marker protein PCNA indirectly through the biotin–streptavidin system to make sure that secondary antibodies were connected completely. Secondly, after the two adjacent sections were stained, one of the sections was stained again with NIR QDs-SA. The other one was not stained with any labels. Finally, the two sections were locked with glycerol. After that this step was repeated by reversing the staining order of the two kinds of QDs as control.

3. Results and discussion

3.1. Hadamard transform spectra and fluorescence imaging of NIR QDs labeled gastric tumor tissues

Fig. 1 shows the microscopic fluorescence spectrum and HT image of the gastric cancer tissue (positive sample) and spectrum of normal gastric tissue (negative control) probed by NIR QDs immunofluorescence staining. Curve a shows the fluorescence spectrum of 710 nm QDs probed CK. Curve b shows the spectrum of normal gastric tissue, which clearly exhibits the autofluorescence background from the tissue itself. Curve c, which is the pure fluorescence emission spectrum of CdSeTe QDs probed CK, is produced by subtracting the autofluorescence background (curve b) from curve a. The micrograph in the inset shows the HT fluorescence image of QDs probed CK and it clearly shows that CK locates in the cell membrane, and this is consistent with the expression of CK inside cells. In contrast, the negative control shows no expression of the marker protein (curve b) because no peak at 710 nm appears. These signals can be used as proofs that NIR QDs are fluorescence probes and indeed conjugated to the marker protein CK in tumor tissues.

3.2. Staining titer evaluation between NIR and visible fluorescent QDs probes

In this study, in order to investigate the difference of bioconjugation efficiency between NIR CdSeTe QDs and visible CdSe QDs

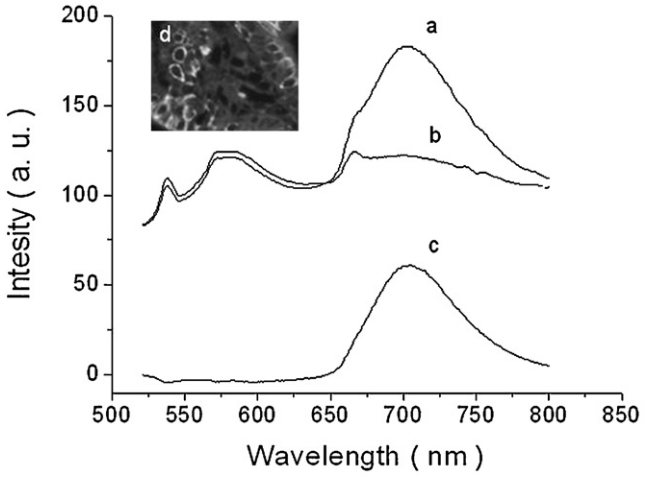

Fig. 1. Fluorescence spectra and image of CK positive and negative gastric cancer specimens probed by NIR QDs immunofluorescent probes. (a) Fluorescence spectrum of positive gastric cancer specimen; (b) autofluorescent background from negative control of (a); (c) the difference spectrum a – b displays only CdSeTe QDs probed CK. The micrograph in the inset shows the HT fluorescence image of the same view-field of (a).

probes when they are used to conjugate marker proteins, we first investigate the concentration gradient staining titer between them for the same biomarkers such as PCNA in the same tissue section. Here, by using the CRi's Nuance multispectral imaging system, the ratio of total QD signal (*S*, counts) and the corresponding area (*A*, pixels) of the signals (*S*/*A*) was used as the staining titer of QDs probes to show their bioconjugation efficiency for cancer biomarkers. The measurement of *S*/*A* allows to quantitatively compare the staining titer between NIR and visible fluorescent QDs probes. The image cubes of eight adjacent sections (each section measured five points) of a same tissue that were stained with these two kinds of QDs-SA at different concentration gradient (100-, 200-, 400- and 800-fold) were captured by the Nuance multispectral imaging system. The staining titer of NIR CdSeTe QDs and visible CdSe QDs probes was obtained and shown in Fig. 2 by quantitative measurements through these image cubes. Clearly, Fig. 2 demonstrates that

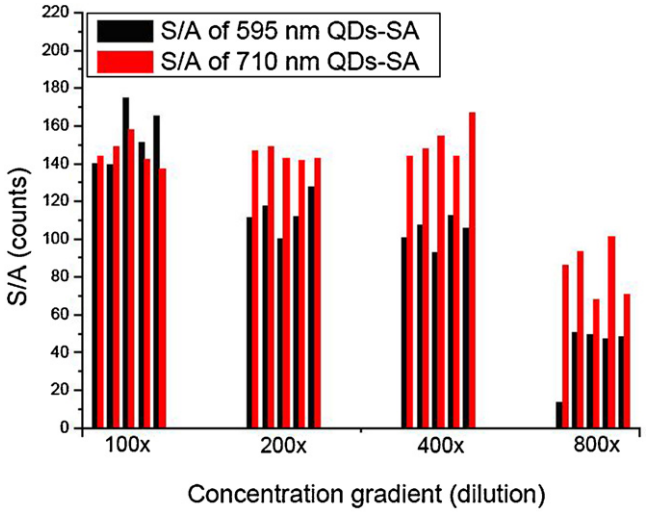

Fig. 2. Column plots depicting staining titer (*S*/*A*) of visible 595 nm (black columns) and NIR 710 nm (red columns) fluorescent QDs probes when the sections (each section measured five points) from the same tissue were stained with the above two kinds of QDs-SA at different concentration gradient (100-, 200-, 400-, and 800-fold dilutions). (For interpretation of the references to color in this figure legend, the reader is referred to the web version of the article.)

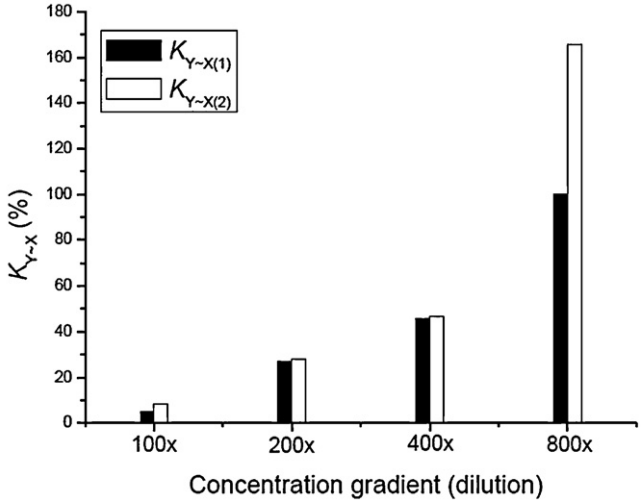

Fig. 3. Scaling relationship of the staining titer between visible QDs and NIR QDs probes at different concentration calculated with $K_{Y\sim X\ (1)}$ and $K_{Y\sim X\ (2)}$.

710 nm QDs is similar to 595 nm QDs at 100-fold dilution in terms of staining titer while 710 nm QDs show higher *S*/*A* than that of 595 nm QDs from 200- to 800-fold dilutions when they are used for immunostaining.

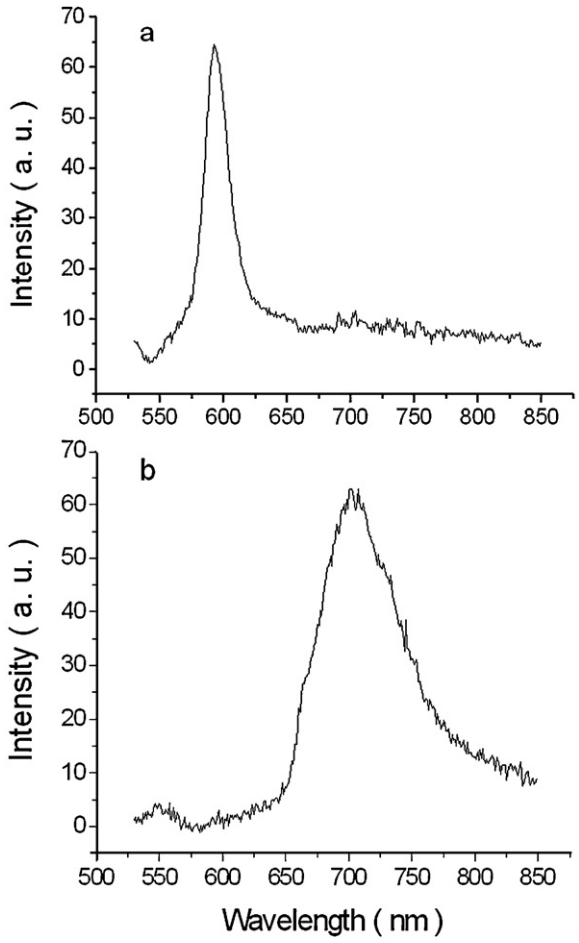

Fig. 4. Fluorescence spectra of PCNA in gastric cancer tissues probed by NIR QDs and visible QDs immunofluorescent probes at 100× dilution. (a) Probed by 595 nm QDs; (b) probed by 710 nm QDs. All the spectra were captured with the HT imaging system. The background of autofluorescence was subtracted from all the spectra.

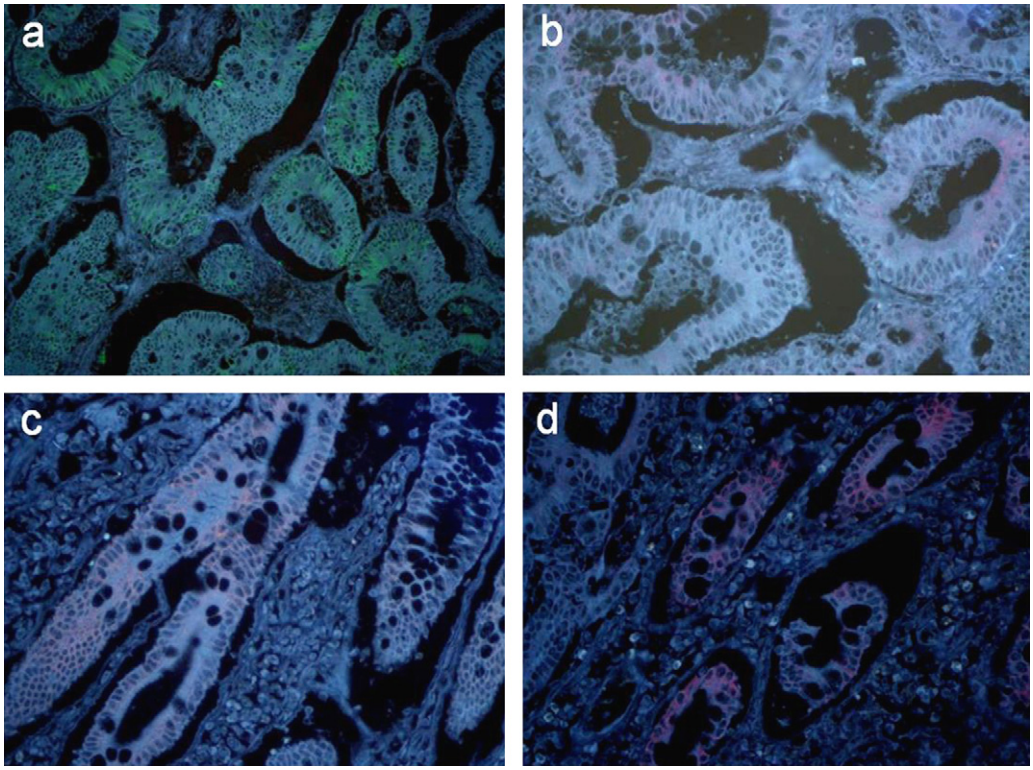

Fig. 5. Fluorescence micrographs of specimens labelled with mixed use of green QDs in visible region and NIR QDs conjugating CK. (a) Probed by QDs-550; (b) probed QDs-710; (c) probed by QDs-710 and QDs-550 (1:1); (d) probed by QDs-710 and QDs-550 (4:1). (For interpretation of the references to color in this figure legend, the reader is referred to the web version of the article.)

The parameter $K_{Y\sim X}$, which measures the difference of the bioconjugation efficiency between the two batches of QDs probes X and Y, is used to evaluate the staining titer between these two kinds of QDs probes. We found that the staining titer of the two kinds of QDs probes are quite similar at 100-fold dilution either by measuring the difference of total five location points' S/A with the following formula, which was described in our previous report [33]:

$$K_{Y\sim X(1)} = \left(\frac{\sum_{i=1}^{5} Y_i}{\sum_{i=1}^{5} X_i} - 1 \right) \times 100\% \quad (1)$$

where 5 is the number of measured locations. The intensity of the individual locations can be used to compare them one by one, or by measuring the difference of total differences of single location point' S/A with the following formula:

$$K_{Y\sim X(2)} = \frac{1}{5} \sum_{i=1}^{5} \frac{Y_i - X_i}{X_i} \times 100\% \quad (2)$$

The scaling relationship of the staining titer between these two kinds of QDs probes at different concentration calculated with the two methods is shown in Fig. 3. With this information, the scaling relationship of the staining titer between any two kinds of QDs can also be easily evaluated, therefore it can be used as the guidance note for the next immunostaing of tumor proteins.

The emission fluorescence spectra of PCNA in gastric cancer tissues probed by NIR QDs and visible QDs immunofluorescent probes at 100-fold dilution, were captured by HT fluorescence spectral imaging microscope and are shown in Fig. 4a and b, respectively, from which we can find that a single peak from QDs-710 or QDs-595 is exhibited and there is little difference between the intensity of their peaks. Therefore, 100-fold dilution was chosen in the following investigation to investigate the competition between NIR QDs and visible QDs.

3.3. Comparison of labeling ability between NIR and visible fluorescent QDs

In this study, in order to investigate the difference between NIR QDs and visible QDs, the specimens were labeled with the mixture of QDs in visible region (550 nm) and NIR QDs-710 to conjugate CK or PCNA in tissues. Fig. 5 shows the fluorescence micrographs of the specimens labeled with NIR QDs, green QDs in visible region, and their mixture of proportion of 1:1 and 4:1 conjugating CK. Fig. 5a and b shows the fluorescence micrographs of the specimens labeled with QDs-550 and QDs-710, respectively. The two fluorescence micrographs show that CK locates in the cell membrane, in green and in red, respectively. Fig. 5c and d shows the fluorescence micrographs of the specimens labeled with the mixture of QDs-550 and QDs-710 in proportion of 1:1 and 4:1 conjugating CK, respectively. These digital micrographs can be used to distinguish whether or not QDs with different colors have already conjugated to the probed proteins in the specimens. Moreover, Fig. 5c and d show that the red signal covers up the green signal. Therefore, we conclude that NIR QDs is much easier to conjugate marker proteins in tissues than visible green QDs, and thus NIR QDs have stronger bioconjugate efficiency in the process of the immunofluorescent staining. In this study, NIR QDs show higher sensitivity than visible QDs when labeling target cancer proteins in tissues, although their concentrations are the same. The difference of bioconjugate efficiency between the two kinds of QDs may be resulted from the different amount of useful functional points of these QDs and the difference of surface condition and steric factor between them.

Although digital photographs can be used to observe whether or not QDs with different colors have already conjugated to the probed proteins in the specimens, the photos based on RGB color format are difficult to accurately distinguish similar colors, even if the emission of red QDs-595 and NIR QDs-710. Therefore, in this case microscopic spectral imaging technique is a suitable tool to

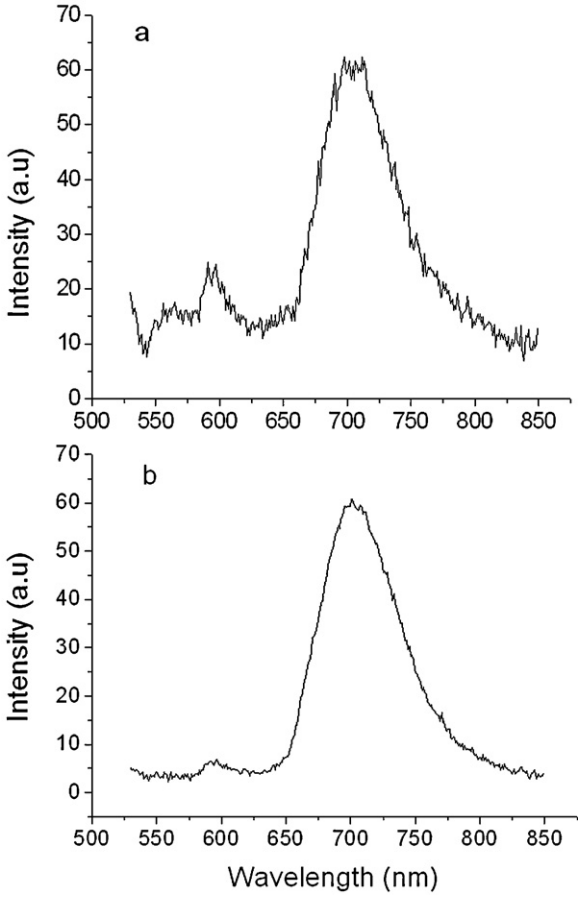

Fig. 6. Fluorescence spectra of PCNA in gastric cancer tissues probed by NIR QDs and visible QDs immunofluorescent probes at different mixing proportions. (a) Probed by QDs-710 and QDs-595 (1:1); (b) probed by QDs-710 and QDs-595 (4:1). All the spectra were captured with the HT imaging system. The background of autofluorescence was subtracted from all the spectra.

efficiently identify the signals from these two kinds of QDs [25]. Fig. 6 shows the HT microscopic fluorescence spectra of PCNA in gastric cancer specimens stained with mixed QDs-595 and QDs-710 in different ratio of concentration with autofluorescence subtracted from the each. Fig. 6a and b are obtained with 1:1 and 4:1 of QDs-710 and QDs-595, respectively. It is worth noting that both spectra show the dominant peak at 710 nm. Therefore, we conclude that NIR QDs are much easier to conjugate marker proteins in tissues than visible QDs, and thus NIR QDs have stronger competitive labeling ability in the process of the immunofluorescent staining. This result can be confirmed by the results obtained by the CRi Nuance multispectral imaging technique. Fig. 7 shows the ratio of staining titer between NIR and visible fluorescent QDs probes at different mixing proportions obtained with the CRi Nuance multispectral imaging technique, and the data matches well with the results by the HT microscopic fluorescence spectra.

Moreover, in order to further verify the competing ability of different kinds of QDs-SA probes when they are used to conjugate marker proteins, the same biomarker PCNA in the same tissue section was repeatedly labeled using QDs-710 and QDs-595. Fig. 8 shows the result of influence of repeated staining with the two kinds of QDs-SA probes. Fig. 8a shows that considerably high NIR fluorescence signal of QDs-710 appears after the QDs-595-treated specimen was counterstained with QDs-710. The intensity of NIR signal is about 20% of that from QDs-595 labeled specimen. In contrast, in Fig. 8b, which shows the result of the reversed staining order of Fig. 8a, only exhibits a very low peak at about 595 nm with

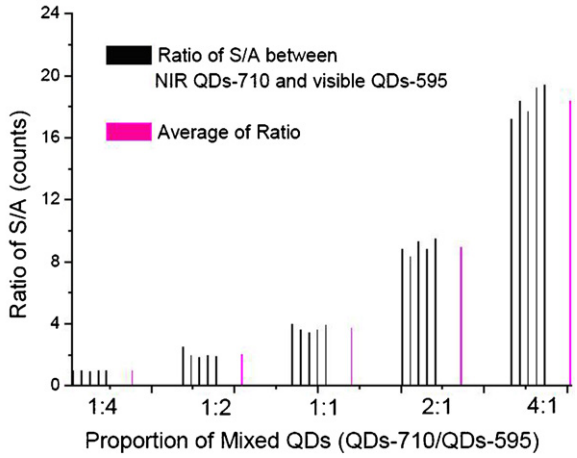

Fig. 7. Ratio of staining titer between NIR and visible fluorescent QDs probes at different mixing proportions.

about 5% of the intensity of the strong NIR signal at 710 nm. The signal from QDs-595 is negligible because it is nearly in the same intensity level of the background noise. This result can be confirmed by the results obtained from the CRi Nuance multispectral imaging technique (data not shown). In addition, the study of PCNA is quite similar to that of CK, and is a further proof that NIR QDs are more sensitive than QDs in visible region when they are simultaneously used to probe the same target molecules in tumor tissues.

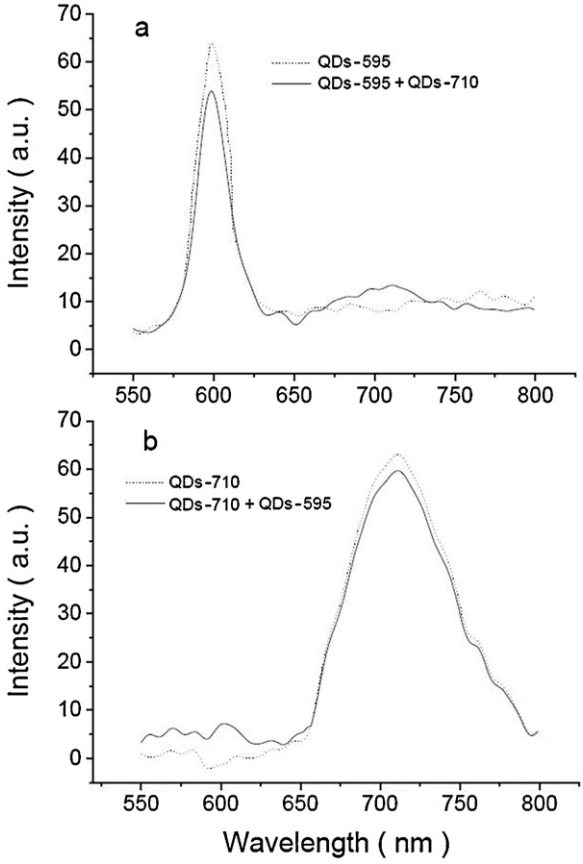

Fig. 8. Comparison of counterstaining in different orders using QDs-710 and QDs-595. (a) The specimen is stained with QDs-595 first and counterstained with QDs-710; (b) the specimen is stained with QDs-710 nm first and counterstained with QDs-595. All the spectra were captured with the HT imaging system. The background of autofluorescence was subtracted from all the spectra.

4. Conclusions

Through the comparison of the labeling ability between NIR CdSeTe/ZnS QDs-SA at 710 nm and visible QDs-SA at 595 nm in immunostaining of marker proteins in gastric cancer tissues, the results demonstrate that the immunostaining ability of NIR QDs probes is stronger than that of visible QDs when the two kinds of QDs coexist. In addition, when the two probes are used for immunostaining successively for the same targeted molecules, staining order has great influence on the final result due to their different bioconjugation efficiency to the marker proteins. Therefore, staining order of different kinds of QDs needs to be taken into account to avoid the interference of the latter QDs on the former one when multiple QDs are used for multicolor labeling. In addition, the results demonstrate that the homemade system of HT spectral imaging can be used as a reliable tool to attain accurate data in biomedical analysis and quantitative evaluation for tumor tissues.

Acknowledgements

This work was supported by the National Basic Research Program of China (973 Program, Nos. 2011CB933600 and 2006CB933100), the Science Fund for Creative Research Groups of NSFC (Nos. 20621502 and 20921062), the National Natural Science Foundation of China (10874135; 20833006; 20875071; 21005056), and the Fundamental Research Funds for the Central Universities (1101015). The authors are grateful to Wuhan Jiayuan Quantum Dots Co., Ltd. for their technical assistances.

References

[1] M.J. Bruchez, M. Moronne, P. Gin, S. Weiss, A.P. Alivisatos, Science 281 (1998) 2013–2016.
[2] W.C.W. Chan, S.M. Nie, Science 281 (1998) 2016–2018.
[3] W.W. Yu, E. Chang, R. Drezek, V.L. Colvina, Biochem. Biophys. Res. Commun. 348 (2006) 781–786.
[4] X. Michalet, F.F. Pinaud, L.A. Bentolila, J.M. Tsay, S. Doose, J.J. Li, G. Sundaresan, A.M. Wu, S.S. Gambhir, S. Weiss, Science 307 (2005) 538–544.
[5] X.H. Gao, L.L. Yang, J.A. Petros, F.F. Marshall, J.W. Simons, S.M. Nie, Curr. Opin. Biotechnol. 16 (2005) 63–72.
[6] F. Pinaud, X. Michalet, L.A. Bentolila, J.M. Tsay, S. Doose, J.J. Li, G. Iyer, S. Weiss, Biomaterials 27 (2006) 1679–1687.
[7] A.M. Smith, S. Dave, S. Nie, L. True, X. Gao, Expert Rev. Mol. Diagn. 6 (2006) 231–244.
[8] R. Weissleder, Nat. Biotechnol. 19 (2001) 316–317.
[9] Y.H. He, R.K. Wang, J. Biomed. Opt. 9 (2004) 200–206.
[10] J.V. Frangioni, Curr. Opin. Chem. Biol. 7 (2003) 626–634.
[11] W. Jiang, A. Singhal, B. Kim, J. Zheng, J. Rutka, C. Wang, W. Chan, J. Assoc. Lab. Autom. 13 (2008) 6–12.
[12] M. Hintersteiner, A. Enz, P. Frey, A.L. Jaton, W. Kinzy, R. Kneuer, U. Neumann, M. Rudin, M. Staufenbiel, M. Stoeckli, K.H. Wiederhold, H.U. Gremlich, Nat. Biotechnol. 23 (2005) 577–583.
[13] R. Weissleder, C.H. Tung, U. Mahmood, A. Bogdanov, Nat. Biotechnol. 17 (1999) 375–378.
[14] A. Zaheer, R.E. Lenkinski, A. Mahmood, A.G. Jones, L.C. Cantley, J.V. Frangioni, Nat. Biotechnol. 19 (2001) 1148–1154.
[15] R.B. Mujumdar, L.A. Ernst, S.R. Mujumdar, C.J. Lewis, A.S. Waggoner, Bioconjug. Chem. 4 (1993) 105–111.
[16] I. Hilger, Y. Leistner, A. Berndt, C. Fritsche, K.M. Haas, H. Kosmehl, W.A. Kaiser, Eur. Radiol. 14 (2004) 1124–1129.
[17] A.P. Alivisatos, W.W. Gu, C. Larabell, Annu. Rev. Biomed. Eng. 7 (2005) 55–76.
[18] S. Kim, Y.T. Lim, E.G. Soltesz, A.M.D. Grand, J. Lee, A. Nakayama, J.A. Parker, T. Mihaljevic, R.G. Laurence, D.M. Dor, L.H. Cohn, M.G. Bawendi, J.V. Frangioni, Nat. Biotechnol. 22 (2004) 93–97.
[19] N.Y. Morgan, S. English, W. Chen, V. Chernomordik, A. Russo, P. Smith, A. Grand-jbakhche, Acad. Radiol. 12 (2005) 313–323.
[20] W.B. Cai, D.W. Shin, K. Chen, O. Gheysens, Q. Cao, S.X. Wang, S.S. Gambhir, X. Chen, Nano Lett. 6 (2006) 669–676.
[21] B. Ballou, B.C. Lagerholm, L.A. Ernst, M.P. Bruchze, A.S. Waggoner, Bioconjug. Chem. 15 (2004) 79–86.
[22] E.G. Soltesz, S. Kim, R.G. Laurence, A.M. Degrand, C.P. Parungo, D.M. Dor, L.H. Cohn, M.G. Bawendi, J.V. Frangioni, T. Mihaljevic, Ann. Thorac. Surg. 79 (2005) 269–277.
[23] C.T. Stadtlander, J.W. Waterbor, Carcinogenesis 20 (1999) 2195–2208.
[24] J.Y. Deng, H. Liang, D. Sun, D.C. Wang, Y. Pan, Ann. Surg. Oncol. 17 (2010) 1259–1266.
[25] S.N. Naryzhny, Cell Mol. Life Sci. 65 (2008) 3789–3808.
[26] G.L. Moldovan, B. Pfander, S. Jentsch, Cell 129 (2007) 665–679.
[27] D. Hoeller, C.M. Hecker, I. Dikic, Nat. Rev. Cancer 6 (2006) 776–788.
[28] A. Couvelard, J.M. Cauvin, D. Goldfain, A. Rotenberg, M. Robaszkiewicz, J.F. Flejou, Gut 49 (2001) 761–766.
[29] S. Braun, K. Pantel, Med. Oncol. 16 (1999) 154–165.
[30] M. Harwit, N.J.A. Sloane, Hadamard Transform Optics, Academic Press, New York, 1979.
[31] H.W. Tang, M.N. Luo, T. Li, L. Pan, Anal. Sci. 22 (2006) 701–707.
[32] H. Xu, J. Peng, H.W. Tang, Y. Li, Q.S. Wu, Z.L. Zhang, G. Zhou, C. Chen, Y. Li, Analyst 134 (2009) 504–511.
[33] H. Xu, C. Chen, J. Peng, H.W. Tang, C.M. Liu, Y. He, Z.Z. Chen, Y. Li, Z.L. Zhang, D.W. Pang, Appl. Spectrosc. 64 (2010) 847–852.